Inorganic Chemistry Communications 180 (2025) 114953

Contents lists available at ScienceDirect

Inorganic Chemistry Communications

journal homepage: www.elsevier.com/locate/inoche

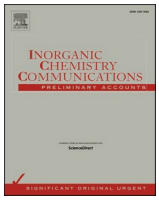

Research Article

Boron nanoparticle doped PVA polymer composite nanofibers: In vitro behaviors

Nilüfer Evcimen Duygulu [a,*], Merve Balkas [b], Fatih Ciftci [c,d,e,*], Mine Kucak [f]

[a] Faculty of Chemical and Metallurgical Engineering, Department of Metallurgical and Material Engineering, Yildiz Technical University, Istanbul, Turkey
[b] Faculty of Engineering, Department of Metallurgical and Materials Engineering, Istanbul University-Cerrahpasa, Turkey
[c] Faculty of Engineering, Department of Biomedical Engineering, Fatih Sultan Mehmet Vakıf University, Istanbul, Turkey
[d] BioriginAI Research Group, Department of Biomedical Engineering, Fatih Sultan Mehmet Vakıf University, Istanbul, Turkey
[e] Department of Technology Transfer Office, Fatih Sultan Mehmet Vakıf University, Istanbul, Turkey
[f] Department of Molecular Biology and Genetics, Istanbul, Yildiz Technical University, Turkey

ARTICLE INFO

Keywords:
Boron nanoparticle
Composite nanofiber
Antimicrobial
Cytotoxicity
Wound dressing

ABSTRACT

This study aims to address the limitations associated with boron sources that contain chemical impurities and to enhance the applicability of boron (B) nanoparticle-doped polyvinyl alcohol (PVA) composite nanofibers in biomedical applications using the electrospinning technique. Morphological analyses conducted through Scanning Electron Microscopy (SEM) and Transmission Electron Microscopy (TEM) confirmed uniform dispersion of B nanoparticles, with an average fiber diameter of 185.52 ± 38.86 nm at a flow rate of 1 mL/h and an applied voltage of 9 kV. X-ray Diffraction (XRD) and TEM indicated the presence of rhombohedral crystalline B nanoparticles, while Fourier Transform Infrared Spectroscopy (FT-IR) revealed enhanced molecular interactions and the formation of new functional groups. Thermogravimetric Analysis (TGA) demonstrated an increase in the thermal stability of the PVA/B composite nanofibers. Water absorption and enzymatic degradation analyses showed that B nanoparticle doping accelerated lysozyme-induced degradation. Antibacterial activity tests exhibited distinct inhibition zones against *E. coli* (13.90 mm), *S. aureus* (6.34 mm), and *C. albicans* (21.30 mm). Biocompatibility evaluation using the MTT assay revealed a high cell viability rate of approximately 99.2 %, confirming the cytocompatibility of the composite fibers. Overall, the findings highlight the promising potential of PVA/B composite nanofibers as multifunctional materials for advanced wound care systems.

1. Introduction

Nanofiber technology is centered on the production of fibers with diameters in the nanometer range. These ultrafine fibers possess a high surface area-to-volume ratio and exceptional porosity, endowing them with unique physical and chemical properties. Consequently, nanofibers are highly versatile and applicable across a broad spectrum of fields. Their outstanding characteristics have garnered significant interest for use in textiles, biomedical engineering, filtration, energy storage, and environmental remediation. The most commonly used method for producing nanofibers is electrospinning due to its accessibility and adaptability [1].

A notable advancement in electrospun nanofibers is the development of composite nanofibers that incorporate nanoparticles along with polymers. Among various polymers, polyvinyl alcohol (PVA) is particularly noteworthy due to its biocompatibility, chemical resistance, excellent film-forming properties, and water solubility [2]. The addition of nanoparticles to PVA-based composite nanofibers enhances their structural, chemical, and antimicrobial properties. The most commonly used nanoparticles in the production of PVA-based composite fibers are silver (Ag) [3,4], zinc oxide (ZnO) [5,6], and titanium dioxide (TiO_2) [7,8].

Nevertheless, ongoing research continues to explore alternative nanomaterials that can further expand the functionality and application areas of PVA-based composite nanofibers. In this regard, boron (B) nanoparticles have recently attracted considerable attention owing to their distinctive physicochemical properties. These include high thermal stability, improved mechanical strength, and notable antimicrobial

* Corresponding authors at: Faculty of Engineering, Department of Biomedical Engineering, Fatih Sultan Mehmet Vakıf University, Istanbul, Turkey (F. Ciftci); Faculty of Chemical and Metallurgical Engineering, Department of Metallurgical and Material Engineering, Yildiz Technical University, Istanbul, Turkey (N. Evcimen Duygulu).
E-mail addresses: nevci@yildiz.edu.tr (N. Evcimen Duygulu), fciftci@fsm.edu.tr, faciftcii@gmail.com (F. Ciftci).

https://doi.org/10.1016/j.inoche.2025.114953
Received 14 April 2025; Received in revised form 4 June 2025; Accepted 21 June 2025
Available online 24 June 2025
1387-7003/© 2025 Elsevier B.V. All rights are reserved, including those for text and data mining, AI training, and similar technologies.

activity. Numerous studies have demonstrated that boron exhibits antibacterial properties effective against Gram-positive and Gram-negative bacteria. They can destroy bacteria by disrupting their cell membranes or inducing oxidative stress [9]. Additionally, boron and its compounds have garnered attention for their promising biological and physicochemical properties, making them suitable for tissue engineering applications [10,11]. B contributes to cell proliferation, enhances wound healing, and promotes angiogenesis, which is critical for tissue regeneration [12,13]. Furthermore, B plays a vital role in osteogenesis by stimulating osteoblast activity and aiding in the mineralization processes necessary for repairing bone tissues. These properties make B an attractive additive for scaffolds designed for applications where enhanced cellular activity and rapid tissue repair are essential.

Numerous studies in the existing literature have explored boron doping using boric acid [14–17]. However, the chemical composition of boric acid may introduce undesirable impurities, which could limit its effectiveness in biomedical applications. This study aims to address these challenges by reducing the adverse effects of boric acid and expanding the potential applications of boron in nanoparticle form in the biomedical field, particularly for wound dressing. To achieve this objective, boron was utilized as a doping material in its nanoparticle form for the current study. The characterization of boron nanoparticle-doped PVA composite nanofibers was conducted through a range of morphological and structural techniques, including SEM, HRTEM, and XRD. Additionally, in vitro, antibacterial assays, and cellular studies have provided evidence that this innovative approach enhances the biocompatibility of boron-doped composite nanofibers.

2. Materials and methods

2.1. Preparation and electrospinning process of PVA and PVA/B composite nanofibers

The methodology for preparing a 10 wt% polyvinyl alcohol (PVA) solution is detailed in our prior publication [18]. Nano-sized B (99.55 % purity, Nanografi) was added to the PVA solutions at varying concentrations. The mixtures were stirred using a magnetic stirrer for around 24 h. The electrospinning process was carried out at an applied voltage of 9 kV, with a 15 cm distance maintained between the needle and the collector. The flow rate was systematically varied between 1 and 5 mL/h, while the concentration of boron in the solution was adjusted within the range of 1 % to 4 %.

2.2. Characterization of PVA and PVA/B composite nanofibers

To investigate the morphologies of B nanoparticles and both PVA and PVA/B composite nanofibers, we employed Scanning Electron Microscopy (SEM) using JSM 6335F and JSM 6510LV instruments from JEOL, Japan, as well as Transmission Electron Microscopy (TEM) (JEM 2100, JEOL, Japan). Compositional analysis was performed using Energy-Dispersive Spectroscopy (EDS) with an Oxford Instruments system from the UK, accompanied by INCA software for data analysis.

ImageJ software was used to measure fiber diameters (US National Institutes of Health, Bethesda, Maryland, USA). The average diameter of the B nanoparticle and composite nanofibers were determined from 100 measurements. Additionally, the porosity percentages of the composite nanofibers were determined using the same software.

The viscosity of the solutions was measured with a digital viscometer (DV E, Brookfield AMETEK, USA). Each measurement was taken four times at room temperature (25 °C) to ensure accuracy and repeatability. Before conducting the measurements, all equipment was calibrated and verified for precision.

A Bruker XPERT-PRO diffractometer with a Cu Kα radiation source (wavelength: 1.5406 Å) was used to record X-ray diffraction (XRD) patterns. A 40 mA and 45 kV generator was employed to conduct the tests over a 2θ range of 10° to 80°.

Fourier-transform infrared (FT-IR) spectroscopy was conducted using the FT-IR-4700 Type A from Jasco IR Affinity-1. The KBr pellet method was employed to record spectra in the wavenumber range of 449.333–4000.6 cm^{-1}. In transmittance mode, each spectrum was averaged over 32 scans at a resolution of 4 cm^{-1}, and observations were made using a triglycine sulfate (TGS) detector.

The thermal properties of the samples were evaluated using thermogravimetric analysis (TGA) with a TA Instruments DISCOVERY SDT 650 system. The measurements were carried out under a nitrogen atmosphere, heating the samples from room temperature up to 800 °C at a constant rate of 10 °C/min. Differential thermal analysis (DTA) curves were also obtained from the TGA data.

2.3. Water absorption analysis of PVA and PVA/B composite nanofibers

Fiber samples were sliced into 2 × 2 cm^2 pieces to assess their water permeability, and a precision balance was used to record their initial dry weights. Each composite nanofiber was placed in a 50 mL beaker containing 20 mL of distilled water. The weight of the composite nanofibers was recorded at time intervals of 2, 5, 10, 15, 20, 25, 30, 35, 40, 45, 50, 55, and 60 min after immersion. To measure the water absorbency, the following formula (**Eq. (1)**) was used:

$$Q_2 = (W_2 - W_1/W_1)^* 100 \quad (1)$$

Q_2: Absorbency,
W_1: Initial weight.
W_2: Weight of the wet fiber nanofiber composites.

2.4. Degradation analysis of PVA and PVA/B composite nanofibers

The degradation tests of PVA and PVA/B composite nanofibers in biological media were conducted. A lysozyme enzyme solution was prepared in phosphate-buffered saline (PBS) at a concentration of 1.5 μg/mL. Gravimetric measurements were performed, and the percentage weight loss of the biomaterials was determined. PVA and PVA/B samples were cut to size (1 cm × 1 cm), and initial weights (W_o) were recorded. Ethanol and UV-C sterilization were performed, respectively. Prepared samples were incubated in the prepared lysozyme solution at 37 °C for 1 week and weighed on the 2nd, 5th, and 7th days of incubation. Before each weighing, the materials were washed with distilled water, dried in a freeze-dryer, and weighed (ALPHA 1–2 LD, Christ, Germany). Lysozyme solution was prepared freshly after each weighing. The experiment was performed in triplicate. Mass loss after enzymatic degradation was calculated with the following formula (**Eq. (2)**):

$$Weight\ loss\ (\%) = (W_o - W_t)/(W_0) \times 100 \quad (2)$$

2.5. Antibacterial analysis of PVA and PVA/B composite nanofibers

The pathogenic microorganisms in this study were sourced from Fırat University, Faculty of Veterinary Medicine, located in Elazığ, Turkey. Bacterial analyses were conducted at the Biomaterials Nanotechnology Laboratory (BioriginAI Research Group, Department of Biomedical Engineering at Fatih Sultan Mehmet Vakıf University). Gram-negative *E. coli*, gram-positive bacteria *S. aureus*, and the fungus *C. albicans* were among the pathogens used in antimicrobial tests.

Serial dilutions of PVA and PVA/B composite nanofiber were prepared at 20, 40, 60, and 80 μL volumes. Following the Clinical and Laboratory Standards Institute (CLSI) guidelines, these dilutions were evaluated using the broth dilution method. The minimum inhibitory concentration (MIC) was defined as the lowest concentration of the antimicrobial agent needed to inhibit 95 % of microbial growth compared to a negative control. The antimicrobial efficacy was quantified using **Eq. (3)** to calculate the inhibition proportional factor (A_f) based on the maximum microbial absorbance at 600 nm, measured in the presence (A_P) and absence (A_C) of the tested membranes.

$$A_f(\%) = \frac{A_C - A_P}{A_C} X\,100 \quad (3)$$

The Disk-diffusion method was utilized to determine the antibacterial activity of PVA and composite nanofiber using ampicillin antibiotic (10 μg) as a reference drug. *E. coli* (ATCC 25922) and *S.aureus* (ATCC 25923) suspensions were collected from 18 h nutrient broth cultures, adjusted to 0.5 McFarland standard turbidity (1.5×10^8 CFU/mL) and diluted to the desired bacterial density (1:10). Mueller-Hinton agar plates were inoculated with 0.1 mL of bacterial suspension (1.5×10^6 CFU/mL). The fibers were sterilized via UV irradiation for 2 h and sliced into 5 mm segments placed on the inoculated agar plates. Plates were incubated at 37 °C for 24 h, after which inhibition zones were measured using a digital micrometer. The testing process was thorough, with three groups tested in triplicate to optimize composite nanofiber formulations, and each test was performed three times to ensure the validity of the results.

2.6. MTT assay of PVA and PVA/B composite nanofibers

The Mossman (Mossman, 1983) approach was utilized to evaluate cell viability using the indirect MTT test. In a 96-well plate, L929 fibroblast cells (1×10^4 cells per well) were cultivated and incubated for 24 h in a humidified environment with 5 % CO. The composite nanofibers were subjected to UV-C sterilization for 20 min. After sterilization, they were transferred into a fresh medium and incubated for 24 h at 37 °C. After 24 h, the extraction fluid was filtered through a 0.22-μm pore size filter. Cells were treated with a 1:1 ratio of composite nanofiber extracts. After 24 h of treatment, an MTT solution (Gold Biotechnology®, St. Louis, MO, USA) was added to each well, followed by incubation at 37 °C for three hours. The supernatant was carefully removed, and dimethyl sulfoxide (DMSO) was added to solubilize the formazan crystals. At 570 nm, absorbance was determined with a microplate reader (Biotek, USA).

2.7. Statistical analysis

GraphPad Prism version 10 software (GraphPad Software Inc., San Diego, CA, USA) was used for all statistical analyses, and one-way analysis of variance (ANOVA) was performed. The mean ± standard deviation (SD) is displayed. We conducted multiple comparison tests to assess statistical differences between groups, including Tukey's and Dunnett's. In every analysis, a *p*-value of less than 0.05 was considered statistically significant.

3. Result and discussion

3.1. Morphological investigation of B nanoparticle, PVA and PVA/B composite nanofibers

Fig. 1 presents the morphological characteristics, particle size distribution, and elemental composition of B nanoparticles. The TEM image presented in Fig. 1**-a** demonstrates that the nanoparticles are spherical and exhibit a relatively uniform morphology. Through TEM analysis, the particle size distribution illustrated in Fig. 1**-b** indicates that the diameters of the nanoparticles range from 40 to 150 nm, resulting in an average particle size of 88.76 ± 20.82 nm. The SEM images shown in Fig. 1**-c** further corroborate the observed distribution and morphology of the boron nanoparticles at a lower magnification. Additionally, the EDS analysis depicted in Fig. 1**-d** confirms the exclusive detection of the boron element within the sample.

Fig. 2 displays the SEM images and histogram diagrams of B nanoparticle doped PVA composite nanofibers with B concentrations varying from 1 % to 4 % by weight. The electrospinning process for the PVA/B composite nanofibers was carried out under controlled conditions, with a flow rate of 1 mL/h and an applied voltage of 9 kV. The average fiber diameters measured were 185.57 ± 58.86 nm, 340.97 ± 85.98 nm, and 337.10 ± 70.82 nm for 1 %, 2 % and 4 % wt. B nanoparticle doped fibers, respectively. The results indicate a trend of increasing fiber diameter with higher B content. The diameters showed similarities at 2 % and 4 % B concentrations (Fig. 4**-a**). It is important to note that using a

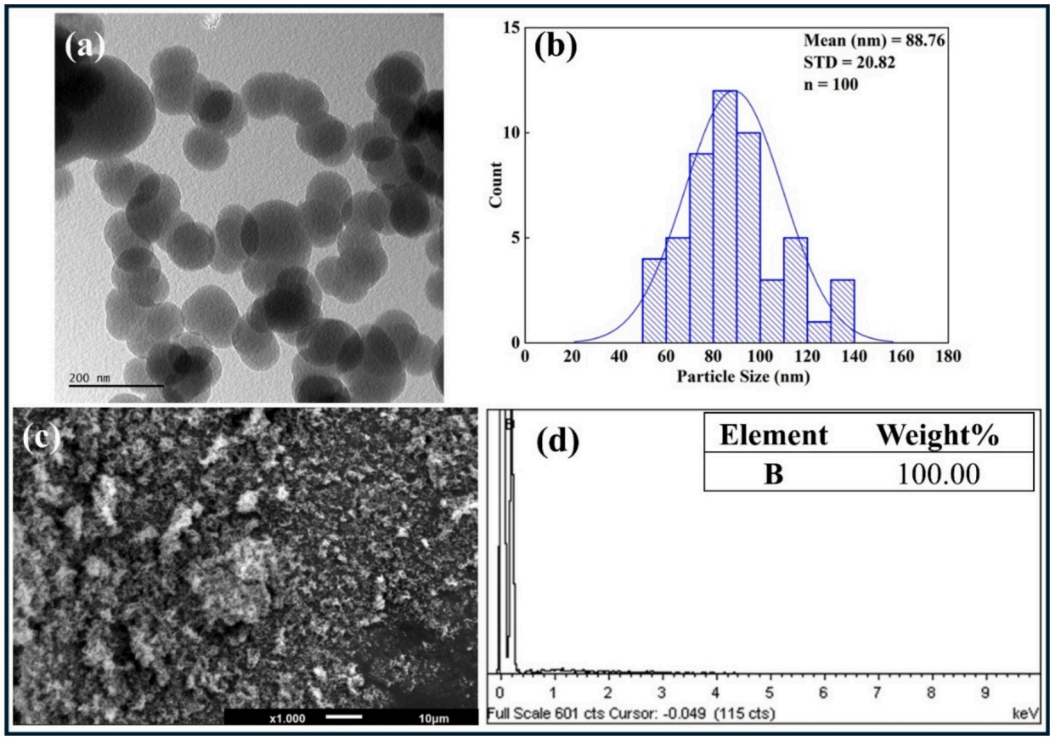

Fig. 1. (a) TEM, (b) particle size distribution (c) SEM (d) EDS spectrum of B nanoparticles.

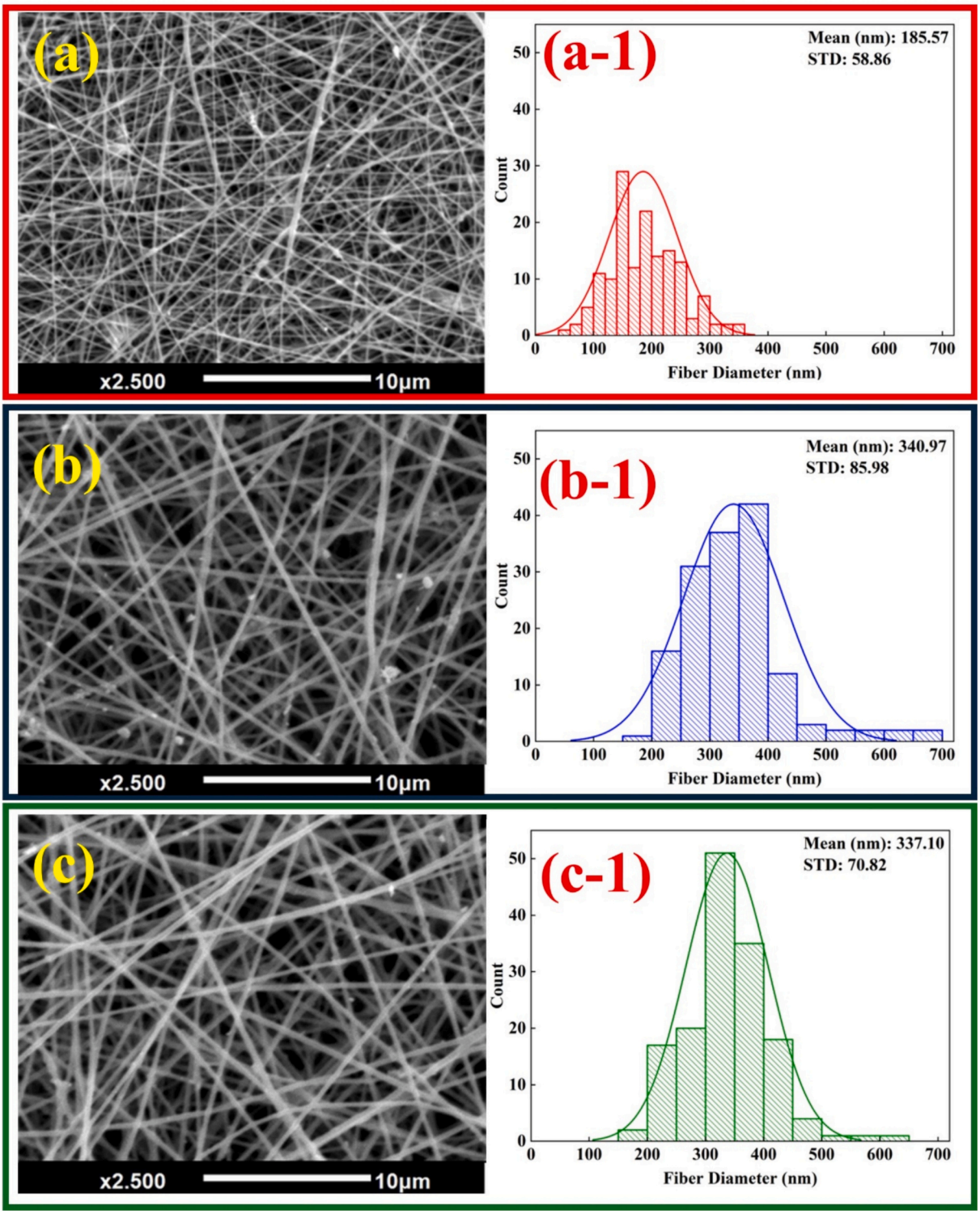

Fig. 2. SEM images and histograms of PVA/B composite nanofibers electrospun at 9 kV and 1 mL/h with different B nanoparticle additions (% wt.): (a) 1, (b) 2, and (c) 4.

high concentration of boron nanoparticles can be economically unfeasible and may lead to dispersion issues. Consequently, experimental studies were primarily conducted with 1 % and 2 % by weight of nanoparticle addition.

Flow rate variation is another crucial parameter for achieving a uniform fiber distribution during electrospinning, as it directly affects fiber morphology, diameter, and consistency. This study systematically varied the flow rates of PVA/B composite nanofibers from 1 mL/h to 5 mL/h for both 1 % and 2 % wt. B concentrations to investigate their effects on fiber formation.

Fig. 3 presents SEM images and fiber distribution histograms illustrating how flow rate variation impacts the nanofiber composites with 1 % wt. B content. The results show that while the average fiber diameter remains similar across different flow rates, the standard deviation varies significantly, influencing fiber uniformity. The composite nanofibers exhibited the most uniform distribution at a flow rate of 1 mL/h, with an

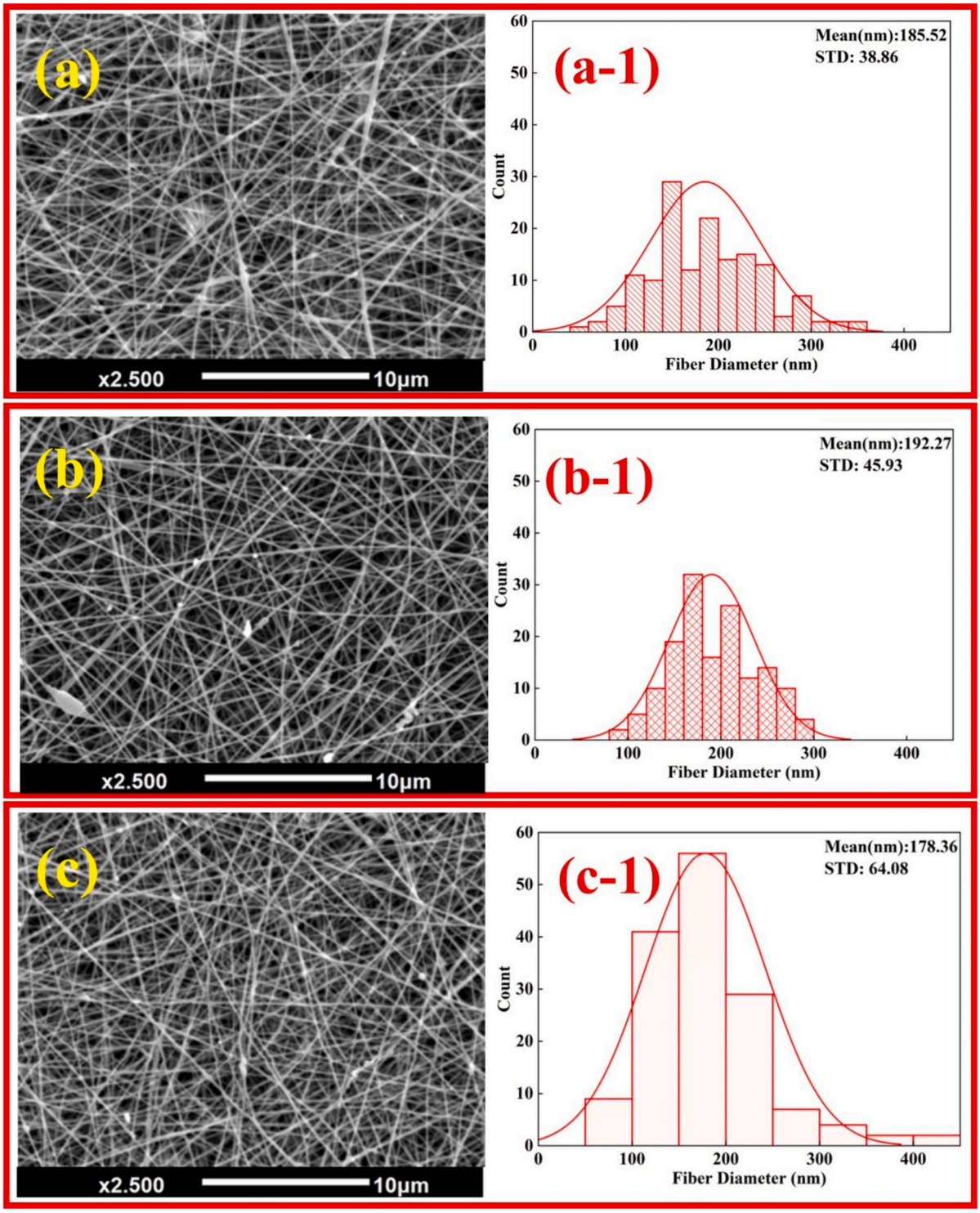

Fig. 3. SEM images and histograms of 1 % wt. B nanoparticle doped PVA/B composite nanofiber electrospun at 9 kV with different flow rates (mL/h): (a) 1, (b) 3, and (c) 5.

average diameter of 185.52 nm and the lowest standard deviation of 38.86 nm.

Fig. 4 illustrates the effect of flow rate variation on SEM and histogram diagrams at 2 % wt. B nanoparticle doped PVA nanofibers. The average fiber diameters were measured at 276.43 ± 52.52 at 1 mL/h, 331.97 ± 67.76 at 3 mL/h, and 405.23 ± 111.80 at 5 mL/h flow rates. These results indicate that as the flow rate increases, the diameter of the composite fibers also increases, confirming a trend identified in previous studies [18].

Fig. 5 presents the statistical analysis of average fiber diameter variations across different flow rates of 1 % and 2 % wt. B content. At 2 % wt. B nanoparticle content, the flow rate significantly influences fiber diameter. Conversely, at 1 % B content, variations in flow rate have a negligible effect on diameter. This ability to control fiber diameter through boron addition is especially beneficial for applications in filtration, biomedical scaffolding, and functional membranes, as the dimensions of the fibers play a crucial role in material performance [19,20]. Additionally, the findings indicate that a lower flow rate leads

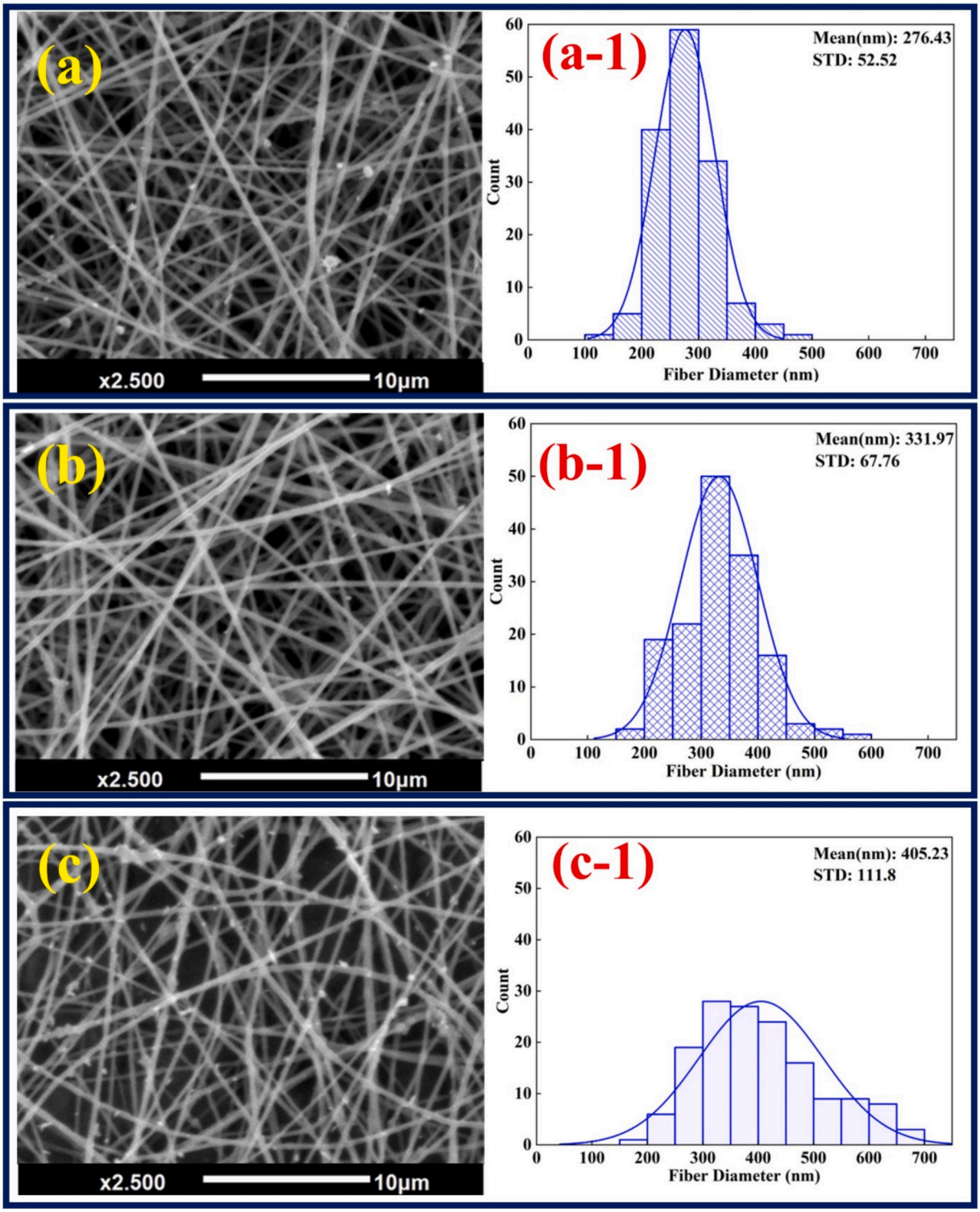

Fig. 4. SEM images and histograms of 2 % wt. B nanoparticle doped PVA/B composite nanofibers electrospun at 9 kV with different flow rates (mL/h): (a) 1, (b) 3, and (c) 5.

to improved fiber uniformity and reduced variability, making it an ideal condition for producing consistent nanofiber structures. Therefore, using 1 % wt. B nanoparticle content with a flow rate of 1 mL/h is optimal for producing PVA/B composite nanofibers.

According to our previous study, the viscosity of the solutions plays a crucial role in fiber distribution and diameter. The viscosity of the 1 wt% B nanoparticle-doped PVA/B composite nanofiber was measured at 46.43 ± 0.27 mPa·s, while the viscosity of PVA was measured at 58.25 ± 5.34 mPa·s. The viscosity of the PVA solution significantly decreases with the blending of B nanoparticles, resulting in a reduction of about 20 %. Additionally, the porosity of the PVA/B composite nanofibers was calculated to be 6.57 % using ImageJ software, which analyzed the SEM images of the samples. In contrast, the porosity of the PVA nanofiber was measured at 7.37 % [18]. The doping of B nanoparticles reduces porosity by filling the voids and altering the fiber morphology.

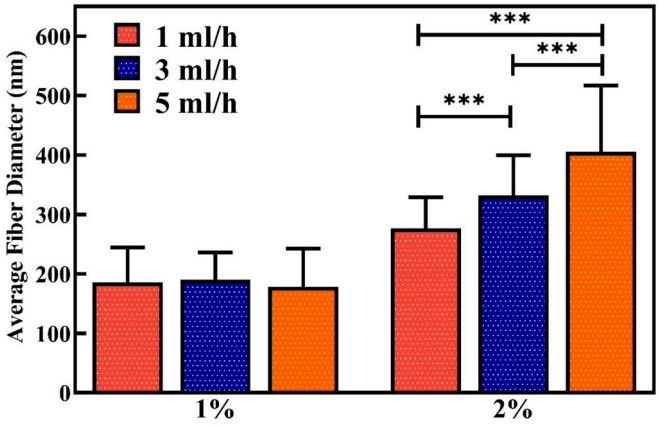

Fig. 5. Average fiber diameter variation of the PVA/B composite nanofibers electrospun at 9 kV, with different B concentrations and flow rates. (Rel. Exp. indicates relative expression, $***P < 0.005$).

Fiber porosity plays a crucial role in the performance and function of biomedical materials [21]. Highly porous fibers enhance cell adhesion, proliferation, and nutrient exchange, making them ideal for applications in tissue engineering, wound healing, and drug delivery. In contrast, materials with lower porosity offer improved barrier properties, which are crucial for protective wound dressings and filtration membranes. These materials effectively prevent microbial infiltration while maintaining sterility [22].

3.2. XRD analysis of PVA and PVA/B composite nanofibers

The XRD analyses of PVA/B composite nanofiber, PVA, and aluminum are shown in Fig. 6. The PVA polymer possesses a semi-crystalline structure, with a notable peak at $2\theta = 29.4°$ corresponding to the (101) crystal plane, marked in blue. All nanofiber composites electrospun onto aluminum foil, with aluminum-related diffraction peaks indicated in green. According to JCPDS # 4–787, the 2θ values for the aluminum diffraction peaks are approximately 38.47°, 44.72°, 65.10°, 78.24°, and 82.45°, representing the crystal planes (111), (200), (220), (311), and (222), respectively. Fig. 6 (marked in red) shows the B nanoparticle-doped PVA composite nanofiber. The analysis identified a rhombohedral structure of alpha B, with the space group R-3 m (166). Intense peaks were observed at the following angles: $2\theta = 44.71°$ for the (202) plane, $2\theta = 57.71°$ for the (211) plane, $2\theta = 65.13°$ for the (030) plane, and $2\theta = 78.24°$ for the (220) plane, matching JCPDS # 78–1571.

3.3. TEM analysis of PVA and PVA/B composite nanofibers

Fig. 7 shows TEM images of the PVA/B composite nanofiber with various magnifications, demonstrating a homogeneous dispersion of nanoparticles without any protrusion. The TEM-EDS spectrum (Fig. 7-**d**) confirms the presence of B nanoparticles in the PVA composite nanofiber.

The selected area electron diffraction (SAED) technique was used in high-resolution transmission electron microscopy (HR-TEM) imaging to analyze the diffraction characteristics of boron nanoparticles in the polyvinyl alcohol (PVA) nanofiber composite. The SAED patterns, shown in Fig. 7-**e**, present a series of concentric rings, confirming that the boron nanoparticles are polycrystalline. The diffraction peaks correspond to the rhombohedral crystal planes (003), (110), and (030), indicating the structural properties of boron in the composite nanofiber.

3.4. FT-IR analysis of PVA and PVA/B composite nanofibers

FT-IR spectra of PVA and PVA/B nanofiber composite nanofibers are shown in Fig. 8. The stretching vibrations of hydrogen-bonded -OH groups are responsible for the broad band observed at 3313 cm^{-1} in PVA [23]. Interactions between PVA chains in the presence of B are shown by the minor shift and decreased intensity of this band in the PVA/B spectra. The band at 2930 cm^{-1}, present in both PVA and PVA/B, corresponds to C—H stretching vibrations [24]. The absence of significant intensity changes suggests that boron incorporation does not affect the C—H bonds. Carbonyl (C=O) stretching vibrations are exhibited by a strong band in the PVA/B spectra at 1726 cm^{-1} [25] [26]. The absence or weakness of this band in the PVA nanofiber indicates that boron doping into the PVA structure has led to the formation of carbonyl groups. The -CH_2 bending and C-O-C asymmetric stretching vibrations in PVA are represented by the bands at 1438 cm^{-1} and 1247 cm^{-1} [27,28]. The effect of boron on the PVA nanofiber is evident in the variations in the intensity and position of these bands in the PVA/B composite nanofiber. Additionally, C—O stretching vibrations in PVA are demonstrated by bands at 1090 cm^{-1} [29–31]. Changes in these bands in the PVA/B spectra further demonstrate the effects of boron additions on the C—O structure.

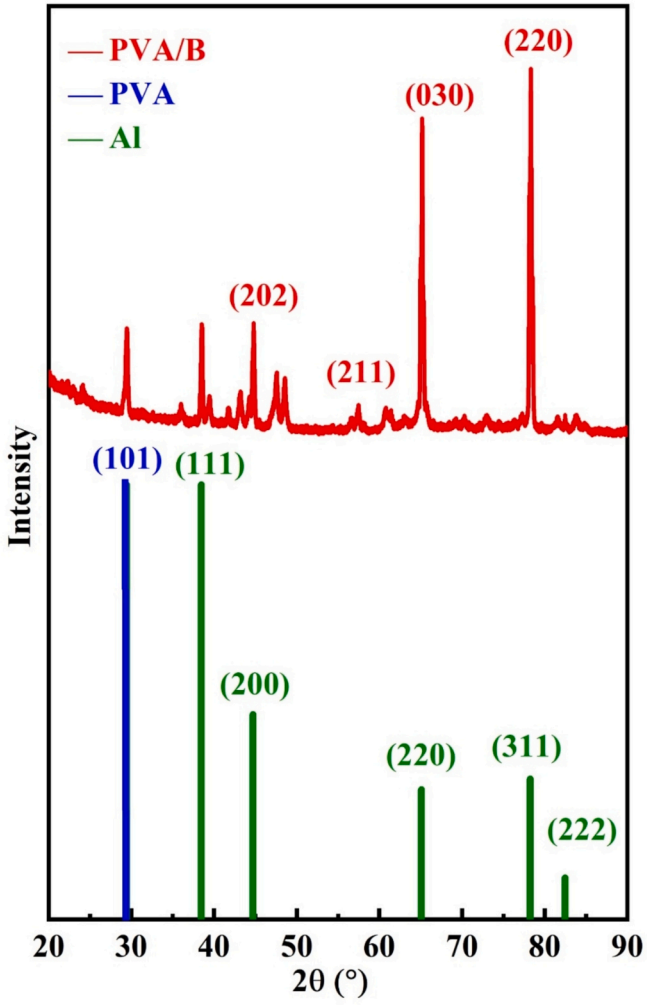

Fig. 6. XRD analysis of PVA/B composite nanofiber (red colored), PVA (blue colored), and aluminum (green colored). (For interpretation of the references to colour in this figure legend, the reader is referred to the web version of this article.)

3.5. TGA analysis of PVA and PVA/B composite nanofibers

TGA and DTG analysis was performed to evaluate the thermal stability and decomposition behavior of PVA and PVA/B composite

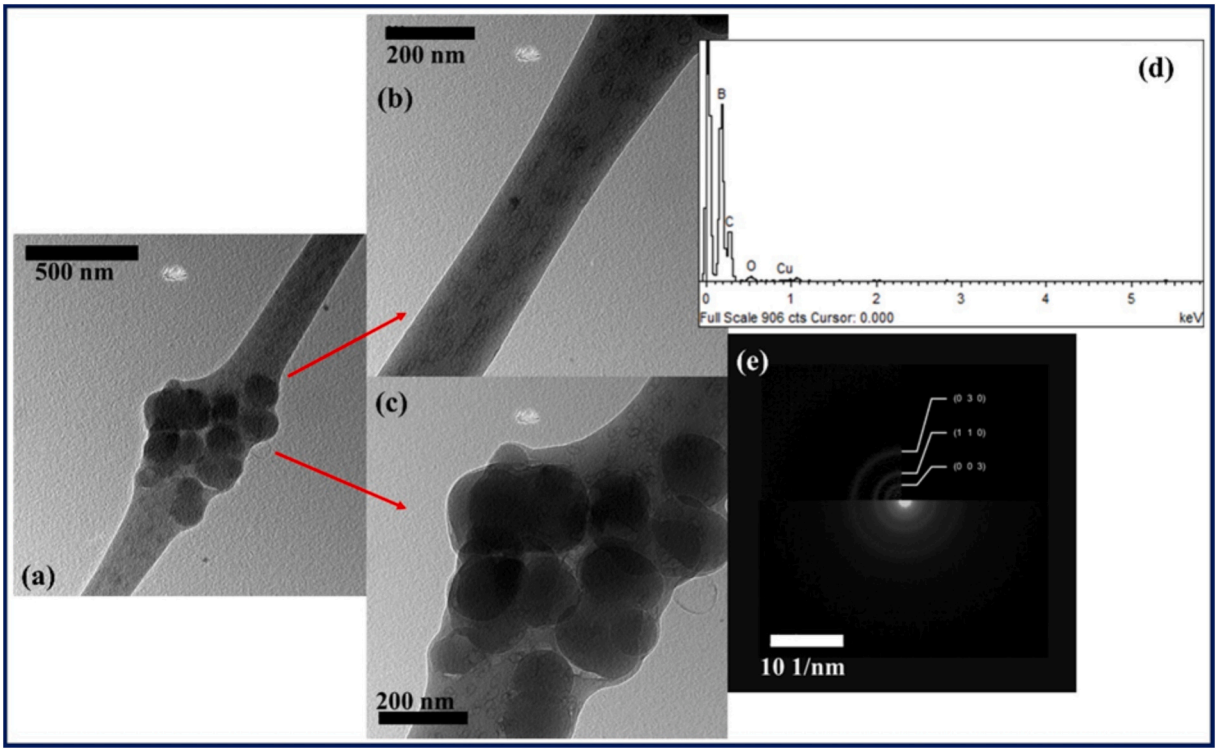

Fig. 7. PVA/B composite nanofiber: (a-b-c) TEM image with different magnifications, (d) TEM-EDS spectrum, (e) Selected area electron diffraction (SAED) pattern and indexation results.

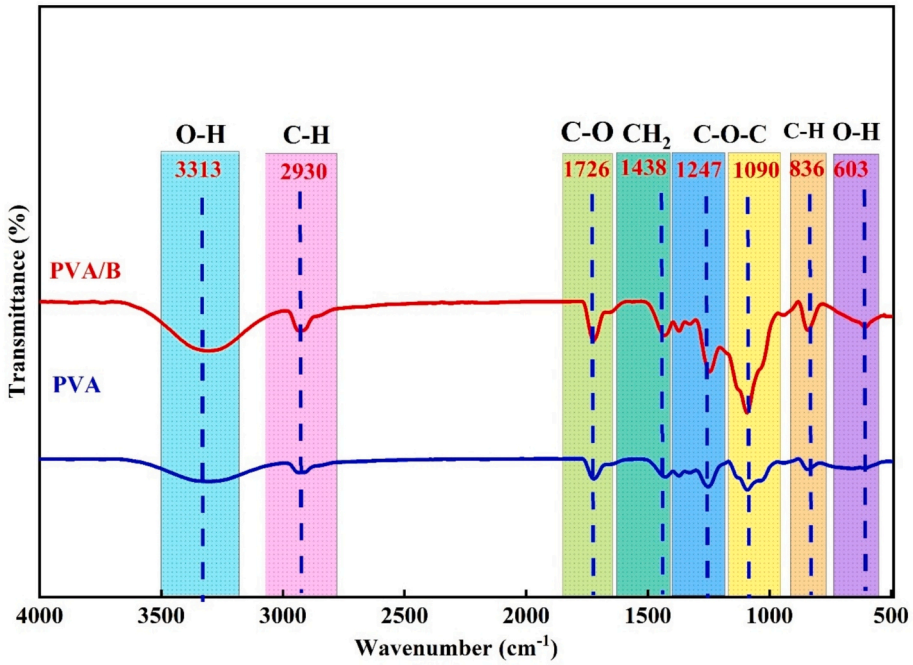

Fig. 8. FT-IR structures of PVA and PVA/B composite nanofibers.

nanofibers. The corresponding TGA and DTG curves are shown in Fig. 9. The TGA curves indicate that the samples undergo a multi-step degradation process. In the initial stage, which occurs below 100 °C, both materials exhibit a slight weight loss of 5.89 % (Fig. 9-**a**). The weight loss for PVA/B is marginally less than that of PVA, primarily due to the evaporation of physically adsorbed water and low-molecular-weight volatiles. Significant weight loss occurs between approximately 200 °C and 400 °C, corresponding to the thermal decomposition of the PVA polymer chains. At this stage, PVA undergoes a significant mass loss of 82.40 %, whereas the PVA/B composite exhibits a lower mass loss of 68.26 %. This reduction in weight loss indicates that the addition of B enhances the thermal stability of the nanofibers by delaying polymer chain scission. In the final decomposition stage (above 400 °C), further degradation of carbonaceous residues occurs. At 800 °C, the residual

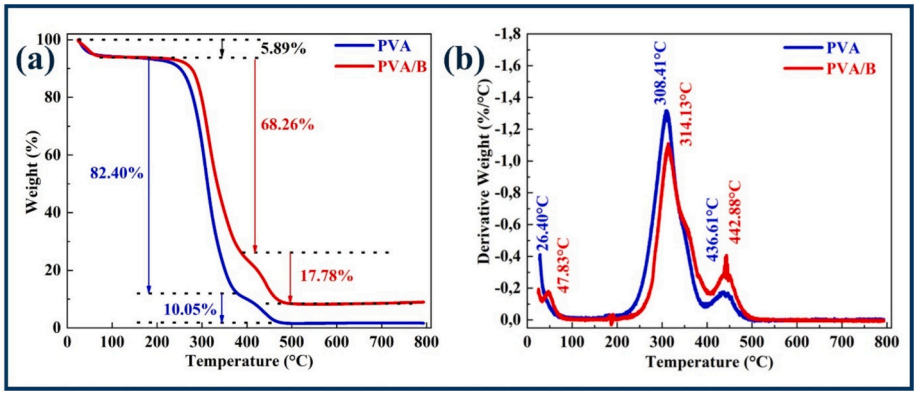

Fig. 9. (a)TGA and (b) DTA curves of PVA and PVA/B composite nanofiber.

char content is 10.05 % for PVA and 17.78 % for the PVA/B composite nanofiber. The higher residue content suggests that B contributes to the formation of thermally stable structures and inhibits complete decomposition. Ozcan et al. have also found similar results, indicating that boron doping enhances oxidation resistance, allowing 30 % of the weight of 0.5 wt% boron-doped fibers to remain above 500 °C, which supports the effective integration of boron.

The DTG curves provide additional insight into the kinetics of decomposition. The first endothermic peak, related to moisture loss, is observed at 26.40 °C for PVA, while it shifts to 47.83 °C for PVA/B. This shift indicates a stronger interaction between the water molecules and the composite matrix. The primary degradation peak also shifts from 308.41 °C in PVA to 314.13 °C in PVA/B, further confirming the enhanced thermal resistance of the PVA/B composite nanofiber. A secondary degradation peak, corresponding to the breakdown of more stable structures, occurs at 436.61 °C for PVA and 442.88 °C for PVA/B (Fig. 9-**b**).

Overall, both TGA and DTG analyses reveal that the addition of B significantly improves the thermal stability of PVA nanofibers. This enhancement can be attributed to the potential interactions between PVA chains and component B, which may limit thermal motion and delay degradation reactions [32].

3.6. Water absorption analysis of PVA and PVA/B composite nanofibers

Fig. 10 illustrates the water absorption percentages of PVA and PVA/B nanofibers. According to the data, the water absorption of the nanofibers showed a decreasing trend over time. The most significant reduction was observed in the PVAB nanofibers, attributed to the hydrophilic characteristics of the B nanoparticle. In comparison, the PVA nanofiber exhibited more excellent resistance to water absorption than the PVA/B composite nanofibers.

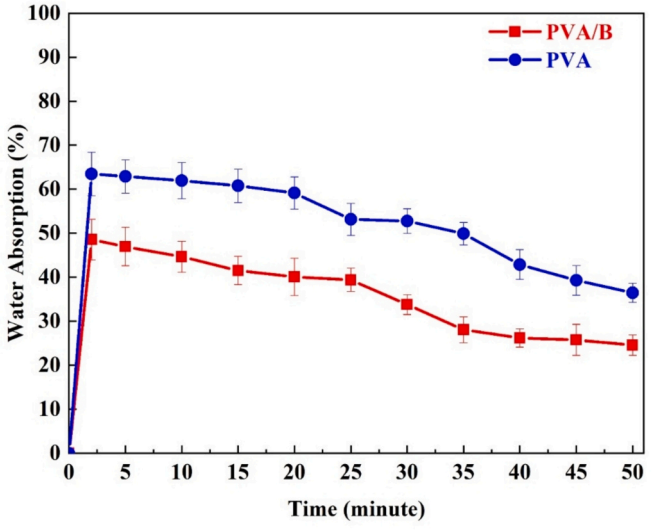

Fig. 10. Water absorbance of PVA, PVA/B composite nanofiber with time variation.

Due to their porous structure, nanofibers can absorb water into their surfaces and pores when submerged. Generally, as the diameters of the fiber increase, the number and size of the pores decrease. Thicker nanofibers create larger pores, resulting in a reduction in the total number of pores [33,34]. These porous properties of nanofibers make them suitable for practical applications such as drug delivery systems, filtration, and tissue scaffolding [19,20]. The formation of thin fiber structures creates a high surface area, facilitating enhanced water passage due to increased porosity.

3.7. Degradation analysis of PVA and PVA/B composite nanofibers

This study evaluated the enzymatic degradation profile of PVA and PVA/B composite nanofibers in a lysozyme medium over time. Fig. 11 presents a graph comparing the mass losses of PVA and PVA/B samples

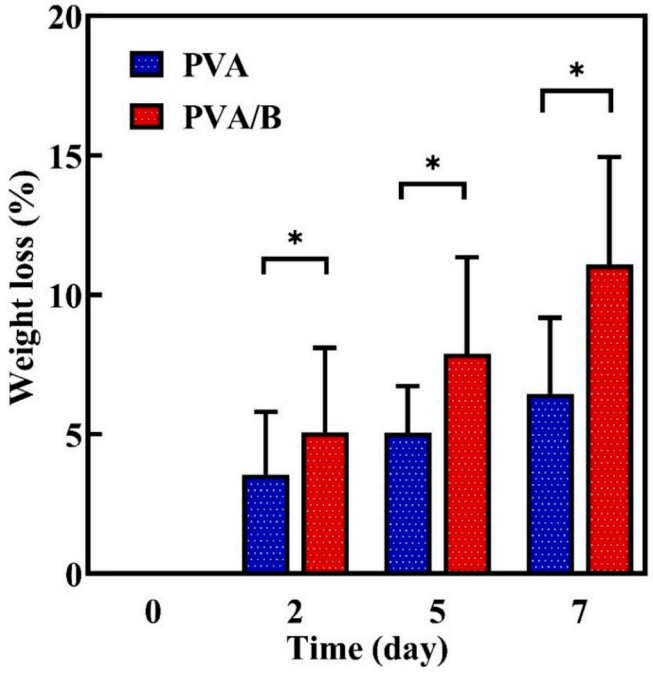

Fig. 11. Weight loss of PVA and PVA/B composite nanofibers time variation.

resulting from enzymatic degradation in the lysozyme medium at 2, 5, and 7 days. Degradation monitoring was conducted through weight measurements on the 2nd, 5th, and 7th days, and average mass loss percentages were calculated.

The findings indicate that the PVA/B nanofibers exhibited significantly greater weight loss than their PVA counterparts across all time points ($P < 0.05$). Especially on day 2, the weight loss in the PVA group was approximately 5 %, while the PVA/B demonstrated a weight loss exceeding 7 %. By day 5, the degradation of PVA was around 8 %, while it reached 11 % in the PVA/B group. The most pronounced difference was observed on day 7, where the average mass loss of the PVA was 12 %, while this value exceeded 15 % in the PVA/B. These data demonstrate that boron nanoparticle doping plays a role in enhancing the degradation of PVA in an enzymatic environment.

A study conducted by Xu et al. [35] examined the in vitro degradation of PVA and chitin-based composite films incorporating anthocyanins in physiological saline solutions, both with and without the presence of lysozyme. Their findings revealed that the inclusion of these additives in the presence of lysozyme significantly enhanced the degradation rate of PVA. Notably, films augmented with anthocyanins exhibited a mass loss of over 66 % within a period of 7 days, whereas PVA films displayed a considerably lower degradation rate. In alignment with these observations, our study demonstrated that the PVA/B composite, formed by adding boron nanoparticles, experienced a greater degree of mass loss compared to PVA.

Furthermore, research published by Xue et al. [36] indicated that boric acid-doped PVA hydrogels possess an elevated water retention capacity and exhibit accelerated degradation at specific concentrations. Consistent with these findings, the current results suggest that boron doping does not consistently function as a "stabilizer." Instead, it may, in specific contexts, facilitate enzymatic access. Specifically, in PVA systems characterized by low crosslink density and an amorphous structure, B doping can engender structural openings that may enhance enzymatic attack.

3.8. Antibacterial analysis of PVA and PVA/B composite nanofibers

The disc diffusion and MIC methods were utilized to evaluate the antimicrobial effects of PVA and PVA/B composite nanofibers against various microorganisms. The disc diffusion method measured inhibition zones for each nanofiber composite against *E. coli, S. albicans*, and *C. albicans*. The results in Table 1 indicate that the inhibition zone values for pure PVA nanofibers were 10.3 mm for *E. coli*, 2.23 mm for *S. aureus*, and 12.75 mm for *C. albicans*. These findings suggest that PVA has a limited antimicrobial effect on these pathogens. In contrast, the PVA/B composite nanofiber exhibited significantly larger inhibition zones against all three microorganisms, specifically 13.9 mm for *E. coli*, 6.34 mm for *S. aureus*, and 21.3 mm for *C. albicans* (Table 1). These results highlight the potent antimicrobial activity of the PVA/B composite nanofiber, particularly against *C. albicans*.

The disc diffusion results demonstrate that the PVA/B composite nanofiber achieved significant inhibition zones against all tested microorganisms, exhibiting the most potent antimicrobial properties.

Table 1
The antimicrobial effectiveness of the tested polymer and composite nanofibers, coded as Control: PVA and PVA/B, was evaluated in both polymerized and unpolymerized forms using the agar well and disc diffusion methods, respectively. Antimicrobial activity was assessed by measuring the inhibition zones in millimeters (mm) with standard deviation (SD).

Disc diffusion method (100 mg/mL)	Multidrug-resistant strains		
	E. coli	*S. aureus*	*C. albicans*
Control: PVA nanofiber	10.30 ± 0.8	2.23 ± 0.01	12.75 ± 0.02
PVA/B composite nanofiber	13.90 ± 0.21***	6.34 ± 0.51***	21.30 ± 1.20***

Statistical analyses of PVA and PVA/B composite nanofibers about *E. coli* (Fig. 12.**a**) and *S. aureus* (Fig. 12.**b**) are presented. The impact on *C. albicans* (Fig. 12.**c**) further emphasizes the potential of this nanofiber composite in combating fungal infections.

The MIC method was employed to evaluate the inhibition efficiency of a nanofiber composite at various concentrations (20 %, 40 %, 60 %, and 80 %) (Table 2). This method assessed the efficacy of the nanofiber composite against different pathogens. The control, composed of PVA fiber, exhibited a maximum inhibition of 34.14 % against *E. coli*, 48.68 % against *S. aureus*, and 63.39 % against *C. albicans*. These results indicate that PVA fiber only demonstrates antimicrobial activity at higher concentrations, with its relatively limited effectiveness.

In contrast, the PVA/B composite nanofiber showed significantly higher inhibition rates against all tested pathogens than PVA. Notably, the PVA/B composite nanofiber achieved a remarkable 92.68 % inhibition rate against *E. coli*, highlighting its potential as an effective agent for combating bacterial infections. Additionally, 60.59 % and 62.94 % inhibition rates were recorded for *S. aureus* and *C. albicans*, respectively, further confirming the broad-spectrum antimicrobial properties of the PVA/B composite nanofiber.

The MIC method results (Fig. 13) indicate that the PVA/B composite nanofiber exhibits strong antimicrobial effects against various pathogen species. Both methods showed that the PVA/B composite nanofiber displayed the most effective antimicrobial activity against microorganisms such as *E. coli*, *S. aureus*, and *C. albicans*. When assessed using the disc diffusion method, this composite nanofiber created large inhibition zones, particularly against fungal infections. It also showed significant inhibition rates against bacterial pathogens in the MIC method. Additionally, the PVA/B composite nanofibers exhibited superior antimicrobial properties compared to PVA. PVA/B composite nanofibers have promising potential for biomedical applications, especially in treating multidrug-resistant bacterial and fungal infections.

3.9. Cell study of PVA and PVA/B composite nanofibers

The findings from the MTT assay are essential for evaluating the biocompatibility of PVA-based nanofiber composites intended for tissue engineering and wound dressing applications. The materials must exhibit minimal toxicity and high cell viability for these purposes. Cell viability rates exceeding 98 % indicate that these materials are suitable for sensitive applications such as wound dressings [23,37]. The PVA/B composite nanofiber demonstrated a cell viability of approximately 99.2 % (Fig. 14).

Additionally, a related study examined PLA-based nano clay, specifically montmorillonite (MMT), known for its antibacterial properties and positive effects on wound healing. This material was modified with trimethyl octadecyl ammonium bromide (TMOD) and boron-based compounds, including boron nitride (BN), zinc borate (ZB), and phenylboronic acid (PBA), to create organomodified MMT (OMMT) nanofibrous polymeric matrices. The cytotoxicity of the resulting PLA-OMMT/B nanofiber composites was assessed using human dermal fibroblasts (NHDF-Ad CC-2511), and no toxic effects were detected [38].

The PVA fiber demonstrated a cell viability of around 99.5 %, confirming that PVA is a biocompatible polymer that does not harm cells. Given PVA's inherent biocompatibility, it can enhance the overall biocompatibility of wound dressings used in tissue engineering and medical applications [39]. The high viability rates of PVA and PVA/B composite fibers, exceeding 99 %, indicate that these materials are non-toxic and suitable for wound dressing applications. However, when using these materials in wound dressings, evaluating their long-term effects on cell viability is essential, as excessive boron content may induce cellular stress and slow healing. Therefore, optimizing boron concentration to improve the biocompatibility of wound dressing formulations is crucial. Overall, this study highlights the potential of PVA/B composite nanofibers for wound dressing applications, demonstrating their safety in cytotoxicity and high cell viability.

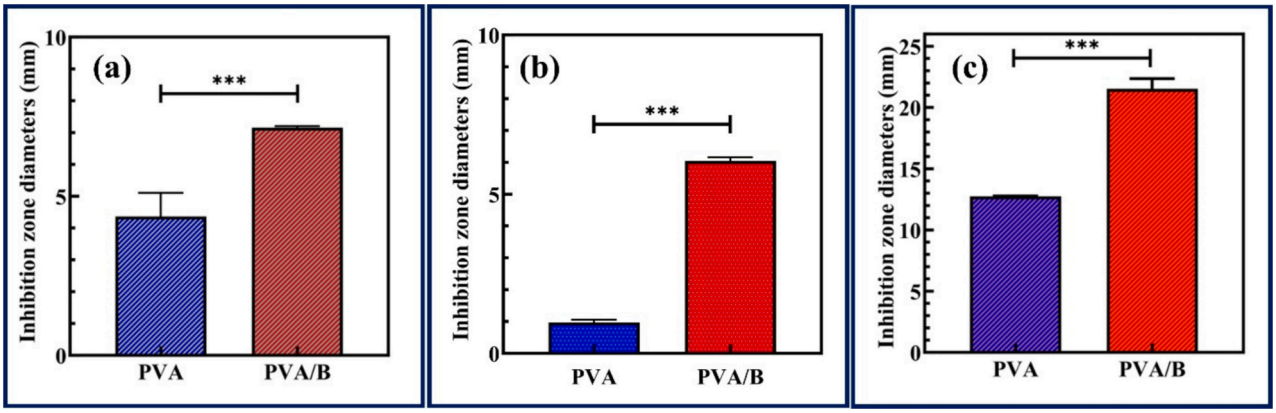

Fig. 12. Inhibition growth graph of PVA and PVA/B composite nanofibers: (a) *E. coli* (b) *S. aureus* and (c) *C. albicans* (mean ± SD values of $n = 5$ independent experiments. ***$P < 0.05$ compared to control. Data were analyzed using a one-way analysis of ANOVA with the Dunnett multiple comparison test.)

Table 2
Detection of the MIC for un-polymerized PVA and PVA/B composite nanofibers (20, 40, 60, 80, and 100 mg/mL) against pathogens by measuring the inhibitory proportional factor (%) (ampicillin (10 μg).

		Minimum inhibitory concentration (MIC) (mg/mL)			
	Pathogens	**20**	**40**	**60**	**80**
Control: PVA nanofiber	***E.coli***	0.0	25.78 ± 1.23	25.07 ± 0.26	34.14 ± 1.01
	S. aureus	0.0	38.09 ± 2.99	34.81 ± 4.07	48.68 ± 3.31
	C.albicans	0.0	49.30 ± 0.95	61.85 ± 3.57	63.39 ± 3.02
PVA/B composite nanofiber	***E.coli***	0.0	53.37 ± 0.58	62.15 ± 3.15	92.68 ± 4.19
	S. aureus	0.0	53.92 ± 0.26	61.25 ± 0.24	60.59 ± 5.21
	C.albicans	0.0	55.12 ± 0.03	63.57 ± 0.7	62.94 ± 0.96

Inhibitory proportional factor (% ± SD).

4. Conclusion

This study successfully demonstrated the fabrication of PVA/B composite nanofibers via electrospinning for wound dressing applications. The use of boron in nanoparticle form improved the structural, thermal, and functional properties of the nanofibers. The optimal electrospinning parameters for the 1 wt% B doped nanofibers were a flow rate of 1 mL/h and an applied voltage of 9 kV.

Characterization analyses confirmed the uniform dispersion of B nanoparticles and the formation of rhombohedral crystalline structures. FT-IR results revealed the development of new functional groups and stronger molecular interactions, while TGA demonstrated improved thermal stability. Doping with B nanoparticles also increased enzymatic degradation by lysozyme due to improved hydrophilicity.

Antibacterial activity tests revealed distinct inhibition zones against *E. coli*, *S. aureus*, and *C. albicans*, indicating broad-spectrum antimicrobial performance. In addition, cytotoxicity evaluations using the MTT assay confirmed excellent biocompatibility, with a cell viability rate of approximately 99.2 %, supporting the material's suitability for biomedical use. Overall, PVA/B composite nanofibers show significant promise as multifunctional wound dressing materials, offering antibacterial efficacy, biocompatibility, and tunable degradability.

CRediT authorship contribution statement

Nilüfer Evcimen Duygulu: Writing – review & editing, Writing – original draft, Visualization, Validation, Supervision, Resources, Methodology, Investigation, Funding acquisition, Formal analysis, Data curation, Conceptualization. **Merve Balkas:** Writing – review & editing, Writing – original draft, Visualization, Validation, Methodology, Investigation, Formal analysis, Data curation, Conceptualization. **Fatih Ciftci:** Writing – review & editing, Writing – original draft, Visualization, Validation, Software, Resources, Project administration, Methodology, Investigation, Formal analysis, Data curation, Conceptualization. **Mine Kucak:** Writing – review & editing, Writing – original draft, Visualization, Validation, Resources, Project administration,

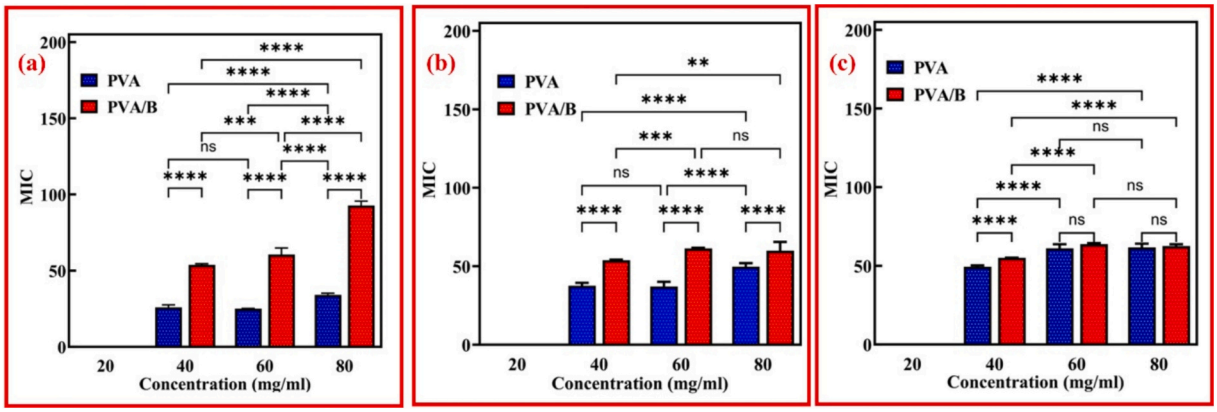

Fig. 13. MIC graph of PVA and PVA/B composite nanofibers: (a) *E. coli* (b) *S. aureus* and (c) *C. albicans* (mean ± SD values of $n = 5$ independent experiments. ****$P < 0.0001$, ***$P < 0.001$, **$P < 0.01$ compared to control. Data were analyzed using a two-way analysis of ANOVA with the Tukey multiple comparison test.)

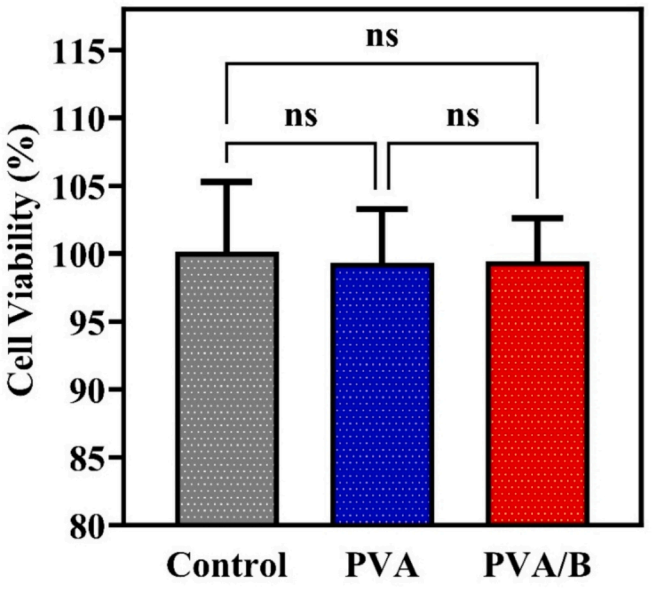

Fig. 14. L929 Cell Viability of PVA and PVA/B composite nanofibers by Indirect Contact Method (mean ± SD values of $n = 3$ independent experiments. $P < 0.05$ compared to control. Data were analyzed using a one-way analysis of ANOVA with the Tukey's multiple comparison test.)

Methodology, Investigation, Formal analysis, Data curation, Conceptualization.

Ethical approval

Not applicable.

Declaration of competing interest

The authors declare that they have no known competing financial interests or personal relationships that could have appeared to influence the work reported in this paper.

Acknowledgements

The work has been supported by the Yildiz Technical University Scientific Research Projects Coordination Department. The project number is FYL-2022-5221.

Data availability

The authors confirm that the data supporting the findings of this study are available within the article. Raw data that support the findings of this study are available from the corresponding author, upon reasonable request.

References

[1] Z.M. Huang, Y.Z. Zhang, M. Kotaki, S. Ramakrishna, A review on polymer nanofibers by electrospinning and their applications in nanocomposites, Compos. Sci. Technol. (2003), https://doi.org/10.1016/S0266-3538(03)00178-7.
[2] A. Altınbay, Effect of concentration on PVA solutions and its usage in recycling carbon fiber/polyamide 12 prepregs 66 (2024) 1693–1699, https://doi.org/10.1515/mt-2024-0110.
[3] Z. Zhang, Y. Wu, Z. Wang, X. Zou, Y. Zhao, L. Sun, Fabrication of silver nanoparticles embedded into polyvinyl alcohol (ag/PVA) composite nanofibrous films through electrospinning for antibacterial and surface-enhanced Raman scattering (SERS) activities, Mater. Sci. Eng. C 69 (2016) 462–469, https://doi.org/10.1016/j.msec.2016.07.015.
[4] T. Uygunoğlu, B. Şimşek, Ö.B. Ceran, Ö. Eryeşil, Novel hybrid fiber reinforced mortar production using polyvinyl alcohol with a blend of graphene oxide and silver nanoparticles, J. Build. Eng. 44 (2021), https://doi.org/10.1016/j.jobe.2021.102641.
[5] M.A. Norouzi, M. Montazer, T. Harifi, P. Karimi, Flower buds like PVA/ZnO composite nanofibers assembly: antibacterial, in vivo wound healing, cytotoxicity and histological studies, Polym. Test. 93 (2021), https://doi.org/10.1016/j.polymertesting.2020.106914.
[6] R. Bouzerara, S. Achour, N. Tabet, S. Zerkout, Synthesis and characterisation of ZnO/PVA composite nanofibres by electrospinning, Int. J. Nanoparticles 4 (2011) 10–19, https://doi.org/10.1504/IJNP.2011.038247.
[7] T.D. Hoang, T.C. Nguyen, T.T. Doan, T.D. Ngo, T.Y. Nguyen, B.T. Ngo, T.T. Tran, T. L. Le, Preparation and photocatalytic and antibacterial properties of polyvinyl alcohol/chitosan/TiO2@ag electrospun nanofibers, Thin Solid Films 797 (2024) 140344, https://doi.org/10.1016/j.tsf.2024.140344.
[8] R. Ekambaram, S. Saravanan, N. Selvam, S. Dharmalingam, Statistical optimization of novel acemannan polysaccharides assisted TiO2 nanorods based nanofibers for skin cancer application, Carbohydrate Polymer Technologies and Applications. 2 (2021), https://doi.org/10.1016/j.carpta.2021.100048.
[9] J. Lv, Y. Qi, Y. Tian, G. Wang, L. Shi, G. Ning, J. Ye, Functionalized boron nanosheets with near-infrared-triggered photothermal and nitric oxide release activities for efficient antibacterial treatment and wound healing promotion, Biomater. Sci. 10 (2022) 3747–3756, https://doi.org/10.1039/d2bm00519k.
[10] P. Balasubramanian, T. Büttner, V. Miguez Pacheco, A.R. Boccaccini, Boron-containing bioactive glasses in bone and soft tissue engineering, J. Eur. Ceram. Soc. 38 (2018) 855–869, https://doi.org/10.1016/j.jeurceramsoc.2017.11.001.
[11] H. Zhang, W.X. Li, S. Tang, Y. Chen, L.M. Lan, S. Li, M. Xiong, X. Hu, Y.H. Liu, J. Sun, G.B. Jiang, A boron-based probe driven Theranostic hydrogel dressing for visual monitoring and matching chronic wound healing, Adv. Funct. Mater. 33 (2023), https://doi.org/10.1002/adfm.202305580.
[12] S. Ahtzaz, T. Sher Waris, L. Shahzadi, A. Anwar Chaudhry, I. Ur Rehman, M. Yar, Boron for tissue regeneration-it's loading into chitosan/collagen hydrogels and testing on chorioallantoic membrane to study the effect on angiogenesis, Int. J. Polym. Mater. Polym. Biomater. 69 (2020) 525–534, https://doi.org/10.1080/00914037.2019.1581202.
[13] Z. Cao, Y. Bian, T. Hu, Y. Yang, Z. Cui, T. Wang, S. Yang, X. Weng, R. Liang, C. Tan, Recent advances in two-dimensional nanomaterials for bone tissue engineering, J. Mater. 9 (2023) 930–958, https://doi.org/10.1016/j.jmat.2023.02.016.
[14] M. Rouhi, F. Garavand, M. Heydari, R. Mohammadi, Z. Sarlak, I. Cacciotti, S. H. Razavi, M. Mousavi, E. Parandi, Fabrication of novel antimicrobial nanocomposite films based on polyvinyl alcohol, bacterial cellulose nanocrystals, and boric acid for food packaging, J. Food Meas. Charact. 18 (2024) 2146–2161, https://doi.org/10.1007/s11694-023-02325-5.
[15] J.H. Woo, N.H. Kim, S. Il Kim, O.K. Park, J.H. Lee, Effects of the addition of boric acid on the physical properties of MXene/polyvinyl alcohol (PVA) nanocomposite, Compos. Part B Eng. 199 (2020), https://doi.org/10.1016/j.compositesb.2020.108205.
[16] W.C. Wu, S.H. Wang, S.T. Ou, Y.W.H. Liu, B.H. Liu, F.G. Tseng, Electrosprayed chitosan/alginate/polyvinyl alcohol nanoparticles as boric acid carriers for 10Boron neutron capture therapy, Nanomedicine 15 (2020) 1067–1077, https://doi.org/10.2217/nnm-2019-0465.
[17] H. Orhan, B. Yilmaz, In vitro properties of electrospun composite fibers containing boric acid and enhanced with epidermal growth factor for wound dressing applications, Fibers and Polymers. 25 (2024) 485–500, https://doi.org/10.1007/s12221-023-00454-8.
[18] N.E. Duygulu, A. Altinbay, F. Ciftci, Antibacterial, mechanical, and thermal properties of ag, ZnO, TiO2 reinforced PVA nanocomposite fibers, ChemistrySelect 9 (2024) e202402311, https://doi.org/10.1002/slct.202402311.
[19] J. Xue, J. Xie, W. Liu, Y. Xia, Electrospun nanofibers: new concepts, materials, and applications, Acc. Chem. Res. (2017), https://doi.org/10.1021/acs.accounts.7b00218.
[20] Z. Zhu, J. Hao, H. Zhu, S. Sun, F. Duan, S. Lu, M. Du, In Situ Fabrication of Electrospun Carbon Nanofibers–Binary Metal Sulfides as Freestanding Electrode for Electrocatalytic Water Splitting, Adv. Fiber Mater. 3 (2021) 117–127, https://doi.org/10.1007/s42765-020-00063-7.
[21] L. Huang, S.S. Manickam, J.R. McCutcheon, Increasing strength of electrospun nanofiber membranes for water filtration using solvent vapor, J. Membr. Sci. 436 (2013) 213–220, https://doi.org/10.1016/j.memsci.2012.12.037.
[22] D. Dharmaraj, N. Chavan, U. Likhitha, U.Y. Nayak, Electrospun nanofibers for dermatological delivery, J. Drug Delivery Sci. Technol. 99 (2024) 105981, https://doi.org/10.1016/j.jddst.2024.105981.
[23] D.G. Özdemir, N. Evcimen Duygulu, A.C. Özarslan, F. Ciftci, Fabrication and characterization of graphene oxide/Fucoidan/chitosan reinforced poly(vinyl alcohol) nanocomposites, J. Mol. Struct. 1301 (2024) 137330, https://doi.org/10.1016/J.MOLSTRUC.2023.137330.
[24] D. Aki, S. Ulag, S. Unal, M. Sengor, N. Ekren, C.C. Lin, H. Yılmazer, C.B. Ustundag, D.M. Kalaskar, O. Gunduz, 3D printing of PVA/hexagonal boron nitride/bacterial cellulose composite scaffolds for bone tissue engineering, Mater. Des. 196 (2020), https://doi.org/10.1016/j.matdes.2020.109094.
[25] A. Fatih Isik, N.O. San Keskin, Y. Ulcay, Synthesis and in vitro antimicrobial characterization of boron-PVA electrospun nanofibers, J. Text. Inst. 110 (2019) 575–580, https://doi.org/10.1080/00405000.2018.1496989.
[26] M. Özcan, C. Kaya, F. Kaya, Cosmic radiation shielding property of boron reinforced continuous fiber nanocomposites produced by electrospinning, Discover Nano. 18 (2023), https://doi.org/10.1186/s11671-023-03940-3.
[27] X. Gao, R. Li, L. Hu, J. Lin, Z. Wang, C. Yu, Y. Fang, Z. Liu, C. Tang, Y. Huang, Preparation of boron nitride nanofibers/PVA composite foam for environmental

remediation, Colloids Surf. A Physicochem. Eng. Asp. 604 (2020), https://doi.org/10.1016/j.colsurfa.2020.125287.
[28] K.S. Lee, K.H. Eom, J.H. Lim, H. Ryu, S. Kim, D.K. Lee, Y.S. Won, Aqueous boron removal by using electrospun poly(vinyl alcohol) (PVA) Mats: a combined study of IR/Raman spectroscopy and computational chemistry, J. Phys. Chem. A 121 (2017) 2253–2258, https://doi.org/10.1021/acs.jpca.6b12578.
[29] E.A. Bursali, S. Coskun, M. Kizil, M. Yurdakoc, Synthesis, characterization and in vitro antimicrobial activities of boron/starch/polyvinyl alcohol hydrogels, Carbohydr. Polym. 83 (2011) 1377–1383, https://doi.org/10.1016/j.carbpol.2010.09.056.
[30] H. Cheng, K. Zhao, Y. Gong, X. Wang, R. Wang, F. Wang, R. Hu, F. Wang, X. Zhang, J. He, X. Tian, Covalent coupling regulated thermal conductivity of poly(vinyl alcohol)/boron nitride composite film based on silane molecular structure, Compos. A: Appl. Sci. Manuf. 137 (2020), https://doi.org/10.1016/j.compositesa.2020.106026.
[31] Y. Kim, J. Kim, Carbonization of polydopamine-coating layers on boron nitride for thermal conductivity enhancement in hybrid polyvinyl alcohol (PVA) composites, Polymers 12 (2020), https://doi.org/10.3390/polym12061410.
[32] M. Özcan, E. Kam, C. Kaya, F. Kaya, Boron-containing nonwoven polymeric nanofiber mats as neutron shields in compact nuclear fusion reactors, Int. J. Energy Res. 46 (2022) 7441–7450, https://doi.org/10.1002/er.7652.
[33] L. Lin, W. Jiang, M. Bechelany, M. Nasr, J. Jarvis, T. Schaub, R.R. Sapkota, P. Miele, H. Wang, P. Xu, Adsorption and photocatalytic oxidation of ibuprofen using nanocomposites of TiO2 nanofibers combined with BN nanosheets: degradation products and mechanisms, Chemosphere 220 (2019) 921–929, https://doi.org/10.1016/j.chemosphere.2018.12.184.
[34] L. Zhou, J. Han, J. Xiao, X. Yang, S. Chen, Microfluidic-assisted self-assembly of 2D Nanosheets toward in situ generation of robust nanofiber film, Small 19 (2023), https://doi.org/10.1002/smll.202301310.
[35] H. Xu, Y. Shi, L. Gao, N. Shi, J. Yang, R. Hao, Preparation and characterization of PH-responsive polyvinyl alcohol/chitosan/ anthocyanin films, Food Sci. Technol. (Brazil). 43 (2023), https://doi.org/10.1590/fst.98022.
[36] H. Xue, Z. Mi, L. Shi, X. Yang, R. Chen, X. Luo, Y. Guan, A high-toughness, tailorable, wearable multifunctional sensor based on multisynergistic fabric-hydrogel constructed via dual-function boric acid bridge, Mater. Today Chem. 33 (2023), https://doi.org/10.1016/j.mtchem.2023.101696.
[37] F. Ciftci, Bioadhesion, antimicrobial activity, and biocompatibility evaluation bacterial cellulose based silver nanoparticle bioactive composite films, Process Biochem. 137 (2024) 99–110, https://doi.org/10.1016/J.PROCBIO.2023.12.021.
[38] S. Asghari Dilmani, S. Koç, D. Çakır, M. Gümüşderelioğlu, Organomodified nanoclay with boron compounds is improving structural and antibacterial properties of nanofibrous matrices, Eur. J. Pharm. Biopharm. 184 (2023) 125–138, https://doi.org/10.1016/j.ejpb.2023.01.015.
[39] O. Tavukcuoglu, N. Evcimen Duygulu, A. Altinbay, F. Ciftci, Green synthesis of silver nanoparticles from Thymus vulgaris and Sambucus nigra extracts in poly (vinyl alcohol) nanofiber matrix: in vitro evaluation, Ind. Crop. Prod. 222 (2024) 119825, https://doi.org/10.1016/J.INDCROP.2024.119825.

Nilufer Evcimen Duygulu, PhD Dr. Nilufer Evcimen Duygulu is an Associate Professor in the Department of Metallurgy and Materials Engineering at Yildiz Technical University in Istanbul, Turkey. She earned her PhD in 2013 and was promoted to Associate Professor in 2025, recognizing her significant contributions to the field. Her research focuses on physical and chemical thin film coating techniques, advanced functional materials, biomaterials, biopolymers, and photovoltaic materials. Dr. Duygulu has numerous publications and has taken part in various national and international research projects. She is also committed to mentoring young scientists and enhancing materials engineering education in Turkey.

Merve Balkas Merve Balkas is a dedicated research assistant at Istanbul University-Cerrahpasa, specializing in the fields of nanomaterials and biomaterials. She earned her master's degree from Yıldız Technical University in 2024, focusing on innovative material science. Currently pursuing her PhD at Istanbul University-Cerrahpasa, Merve's research delves into advanced materials, with a growing emphasis on renewable energy applications.

Fatih Ciftci, PhD Dr. Fatih Ciftci is a researcher at Fatih Sultan Mehmet Vakıf University, Department of Biomedical Engineering (ISTANBUL, TURKEY). He obtained his PhD in the field of bioengineering in 2021. His research interests include biomaterials, biopolymers, bioceramics, hard-soft tissue engineering applications, 3D transdermal tissue scaffold, MXene-MOF-Graphene nanomaterials, wearable technologies, biosensors and rare diseases. He also has projects in the field of artificial intelligence-machine learning, tissue engineering and biotechnology, and his articles will be published in the near future. Dr. Ciftci actively participates in numerous national and international collaborative projects and serves as a reviewer for various scientific journals.

Mine Kucak, PhD Dr. Mine Kuçak continues her research at Yıldız Technical University, Department of Molecular Biology and Genetics (Istanbul, Turkey). She completed her PhD in Molecular Biology and Genetics in 2022. Her academic studies focus on topics such as molecular biology of cancer, angiogenesis, nanobiotechnology, biomaterials, biopolymers, and natural materials. Dr. Kuçak actively participates in numerous research projects, both nationally and internationally.